



**HAL**  
open science

## **Plasma-immersion ion implantation: A path to lower the annealing temperature of implanted boron emitters and simplify PERT solar cell processing**

Adeline Lanterne, Thibaut Desrues, Coralie Lorfeuvre, Marianne Coig, Frank Torregrosa, Frederic Milesi, Laurent Roux, Sébastien Dubois

### ► To cite this version:

Adeline Lanterne, Thibaut Desrues, Coralie Lorfeuvre, Marianne Coig, Frank Torregrosa, et al.. Plasma-immersion ion implantation: A path to lower the annealing temperature of implanted boron emitters and simplify PERT solar cell processing. *Progress in Photovoltaics*, Wiley, 2019, 27 (12), pp.1081-1091. 10.1002/pip.3186 . cea-02570680

**HAL Id: cea-02570680**


**<https://hal-cea.archives-ouvertes.fr/cea-02570680>**

Submitted on 12 May 2020

**HAL** is a multi-disciplinary open access archive for the deposit and dissemination of scientific research documents, whether they are published or not. The documents may come from teaching and research institutions in France or abroad, or from public or private research centers.

L'archive ouverte pluridisciplinaire **HAL**, est destinée au dépôt et à la diffusion de documents scientifiques de niveau recherche, publiés ou non, émanant des établissements d'enseignement et de recherche français ou étrangers, des laboratoires publics ou privés.

# Plasma-immersion ion implantation: A path to lower the annealing temperature of implanted boron emitters and simplify PERT solar cell processing

Adeline Lanterne<sup>1,2</sup>  | Thibaut Desrues<sup>1,2</sup> | Coralie Lorfeuvre<sup>1,2</sup> | Marianne Coig<sup>1,3</sup> | Frank Torregrosa<sup>4</sup> | Frédéric Milési<sup>1,3</sup> | Laurent Roux<sup>4</sup> | Sébastien Dubois<sup>1,2</sup>

<sup>1</sup>University Grenoble Alpes, Grenoble F-38000, France

<sup>2</sup>CEA, Liten, INES, 50 Avenue du Lac Léman, Le Bourget-du-Lac 73375, France

<sup>3</sup>CEA, Leti, MINATEC Campus, 17 rue des Martyrs, Grenoble 38054, France

<sup>4</sup>IBS, Rue Gaston Imbert Prolongée, Z.I. Rousset-Peynier, Peynier 13790, France

## Correspondence

Adeline Lanterne, University Grenoble Alpes, CEA, Liten, Solar Technologies Department Grenoble F-38000, France.  
Email: adeline.lanterne@cea.fr

## Funding information

FUI; Bpifrance

## Abstract

Ion implantation is a suitable and promising solution for the massive industrialization of boron doping, which is a crucial process step for most next-generation solar cells based on crystalline silicon (c-Si). However, the use of ion implantation for boron doping is limited by the high temperature (in the 1050°C range) of the subsequent activation anneal, which is essential to dissolve the boron clusters and reach a high-emitter quality. In this work, we propose the use of plasma-immersion ion implantation (PIII) from B<sub>2</sub>H<sub>6</sub> gas precursor instead of the standard beamline ion implantation (BLII) technique to decrease this temperature down to 950°C. PIII and BLII boron emitters were compared with annealing temperatures ranging from 950°C to 1050°C. Contrary to BLII, no degradation of the emitter quality was observed with PIII implants annealed at 950°C along with a full activation of the dopants in the emitter. At 1000°C, emitter saturation current densities ( $J_{0e}$ ) below 21 fA/cm<sup>2</sup> were obtained using the PIII technique regardless of the tested implantation doses for sheet resistances between 110 and 160 Ω/sq. After metallization steps, the metal/emitter contact resistances were assessed, indicating that these emitters were compatible with a conventional metallization by screen-printing/firing. The PIII boron emitters' performances were further tested with their integration in n-type passivated emitter rear totally diffused (PERT) solar cells fully doped by PIII. Promising results already show a conversion efficiency of 20.8% using a lower annealing temperature than with BLII and a reduced production cost.

## KEYWORDS

annealing temperature, B<sub>2</sub>H<sub>6</sub> plasma, boron doping, n-type PERT solar cells, plasma-immersion ion implantation, silicon solar cells

We report a new way to activate implanted boron emitter at low temperature that is the use of plasma-immersion ion implantation (PIII) from B<sub>2</sub>H<sub>6</sub> plasma. A full activation of the emitter at 950°C was observed even for a high implantation dose corresponding to a sheet resistance of 112 Ω/sq. Promising performances while being integrated in n-PERT solar cells fully doped by PIII were demonstrated with efficiency of 20.8%.

## 1 | INTRODUCTION

The fast evolution and wide range of crystalline silicon (c-Si) solar cell structures, presently under active researches, challenge the prediction of the future industrial transfers that will follow the current switch toward passivated emitter and rear solar cell (PERC).<sup>1</sup> However, near all the considered architectures, such as passivated emitter rear locally diffused (PERL) cell, passivated emitter rear totally diffused (PERT) cell, or interdigitated back contact (IBC) solar cell, with or without passivated contacts, have in common the integration of boron-doped layers. Moreover, boron doping is essential for n-type silicon-based solar cells, which still demonstrate the highest efficiency potential today.<sup>2</sup> Finding a suitable industrial solution for the boron doping is currently one of the keys for the massive industrialization of these next-generation solar cells.

Nowadays, high-temperature gaseous diffusion from  $BBr_3$  or  $BCl_3$  precursors is the main technique used for boron doping. High photovoltaic (PV) conversion efficiencies can be reached by this way with recently 20.8% obtained on a pilot line of screen-printed n-type PERT (n-PERT) solar cells.<sup>3</sup> However, a keen interest toward single-side doping techniques has been seen these past few years.<sup>4</sup> Compared with the double-side doping of the  $BBr_3$  and  $BCl_3$  diffusions, they can strongly simplify the solar cells process flows and thus reduce the production cost of solar cells with boron-doped layers. Most of them have demonstrated high boron emitter electrical qualities such as spin-on coating,<sup>5</sup> screen printing,<sup>4</sup> codiffusion from atmospheric pressure chemical vapor deposition (APCVD) of doped layers,<sup>6</sup> and ion implantation.<sup>7</sup> Some of these single-side doping techniques are already used in high-efficiency n-type solar cells.<sup>8,9</sup>

Among these techniques, this paper focuses on ion implantation, which presents other advantages as the possibility of local doping thanks to an in situ masking<sup>10</sup> that can strongly simplify the process flow of selective emitters and IBC cells, the ability to easily and precisely control the dopant concentration and distribution as well as the high uniformity and reproducibility of the doping.<sup>11</sup> In addition, very high-emitter quality has been reported using a beamline ion implantation (BLII) of  $B^+$  ions, with emitter saturation current densities ( $J_{0e}$ ) lower than  $40 \text{ fA/cm}^2$ ,<sup>12</sup> along with promising PV conversion efficiencies up to 21.8% with screen-printed n-PERT cells.<sup>7</sup>

However, the main drawback of  $B^+$  implantations by the standard BLII technique remains the high annealing temperature ( $\geq 1050^\circ\text{C}$ ) necessary to remove the induced crystal defects as dislocation loops and boron interstitial clusters (BICs)<sup>13,14</sup> and thus achieve low  $J_{0e}$  values.<sup>15</sup> This high-temperature treatment can affect the bulk charge carrier lifetime of Czochralski (Cz) wafers by the formation of oxygen-related defects and by increasing the risk of parasitic contamination (eg, from the furnace). This high-thermal budget also leads to deep emitter profiles and to an increased processing cost. To solve this issue, two approaches have been previously reported. The first, investigated by J. Krügener et al, uses the implantation of  $BF^{2+}$  ions instead of  $B^+$  to reduce the activation annealing temperature thanks to an amorphization of the silicon surface.<sup>12</sup> Activation temperatures as low as  $950^\circ\text{C}$  have been successfully tested, but the solar cell

performances are reduced compared with  $B^+$  implants.<sup>7</sup> The second approach, reported by R. Müller et al, aims at using a very low implantation energy (1–5 keV) to locate the defects closer to the front surface, combined (after the activation step) with a chemical etch back of the first 35 to 85 nm of the boron emitter.<sup>16</sup>

In this work, we studied a third way to activate boron-implanted emitters at temperatures below  $1050^\circ\text{C}$ , the use of plasma-immersion ion implantation (PIII) from  $B_2H_6$  gas precursor. The PIII technique, which presents advantages in capital investment and running cost compared with BLII,<sup>17</sup> also leads to a different as-implanted B concentration ([B]) profile. Whereas BLII implants monoenergetic ions resulting in a Gaussian-type [B] profile, where the depth of the [B] peak directly depends on the implantation energy, PIII can be considered as a multienergetic implant. Indeed, the wafer is directly immersed in the ionic bath where many collisions occur. As a consequence, the dopant concentration profile is shallower (for similar implantation dose and acceleration voltage) and exhibits a maximum always located at the surface level (cf Figure 1). Even if after annealing, a similar doping profile can be obtained, the shallower as-implanted dopants and defects profiles obtained by PIII should allow an easier defect recovery and thus a higher quality of the junction.

The paper aims at comparing BLII and PIII techniques for the boron emitter formation with activation annealing temperatures ranging from  $950^\circ\text{C}$  to  $1050^\circ\text{C}$ . The results include a detailed analysis of the inactive [B], followed by a discussion of the electrical performance variations. The impact of the implantation dose was later studied in the case of PIII implants allowing to compare various emitter sheet resistances. The study also aims at exploring the potential of PIII boron emitters for n-PERT silicon solar cells. Therefore, the contact on these emitters by a conventional screen-printed paste was investigated, and n-PERT silicon solar cells, fully doped by the PIII technique, were processed.

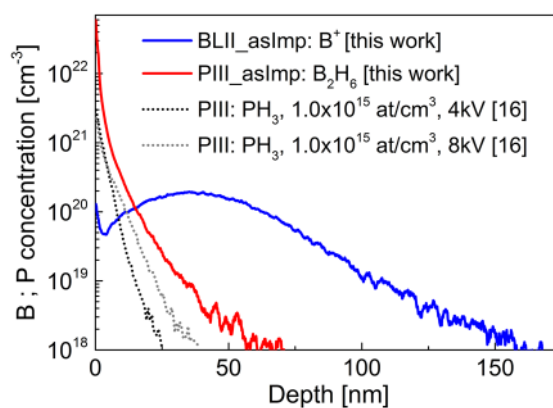


**FIGURE 1** As-implanted boron and phosphorus concentration profiles measured by secondary-ion mass spectroscopy (SIMS). Gaussian profile of beamline ion implantation (BLII) implant of  $B^+$  ions at 10 keV and  $1.2 \times 10^{15} \text{ at/cm}^2$  (BLII\_asImp) compared with plasma-immersion ion implantation (PIII) implants from  $B_2H_6$  and  $PH_3$  gas precursors with two different implantation energies in the  $PH_3$  case, 4 and 8 kV (SIMS from Michel et al<sup>18</sup>) [Colour figure can be viewed at [wileyonlinelibrary.com](http://wileyonlinelibrary.com)]

## 2 | MATERIAL AND METHODS

### 2.1 | Study of implanted boron emitter

**Polished samples** were used to study the [B] profile and boron activation rate after the annealing of BLII and PIII implantations. n-type Cz silicon 239-cm<sup>2</sup> wafers were used for the process of eight different samples, summarized in Table 1. After the wafer polishing in a KOH solution, boron ions were implanted on the front side by the BLII (using a VIISTA® beamline ion implanter from AMAT) or the PIII (using PULSION-SOLAR® tool from IBS) technique. In the case of BLII, B<sup>+</sup> ions were implanted at 10 keV with an implantation dose of  $1.2 \times 10^{15}$  at/cm<sup>2</sup>. For the PIII technique, different doses (from  $1 \times 10^{15}$  to  $5.5 \times 10^{15}$ /cm<sup>2</sup>) were implanted from a B<sub>2</sub>H<sub>6</sub> plasma.

Notice that for the PIII technique, the total implanted ions dose (called machine dose) differs from the boron-implanted dose as the first sums all the implanted ions from the B<sub>2</sub>H<sub>6</sub> plasma (B<sup>+</sup>, H<sup>+</sup>, B<sub>2</sub>H<sub>x<6</sub><sup>+</sup>, and BH<sub>x</sub><sup>+</sup> ions). Depending on the plasma parameters, which can change the complexes dissociation, an identical machine dose can correspond to different boron doses. In this study, two different plasma conditions were used. For the sake of clarity, the machine doses of the first plasma will be noted as multiple of D<sub>0</sub>, and the machine doses of the second plasma will be noted as multiple of D<sub>1</sub>. D<sub>0</sub> and D<sub>1</sub> correspond to the same  $1 \times 10^{15}$  cm<sup>-2</sup> total implanted ions dose but to different implanted boron doses.

To activate the implanted boron, an anneal in a standard horizontal oxidation furnace was performed under N<sub>2</sub> with a plateau of 5 minutes at 1050°C or 30 minutes at 950°C, followed or not by an in situ thermal oxidation step at lower temperature (720°C). The total [B] profiles were obtained by secondary-ion mass spectroscopy (SIMS) measurements following the implantation step (see Figure 1) and following the activation annealing. The oxygen signal was also recorded to estimate the SiO<sub>2</sub> thickness at the surface. Electrochemical capacitance voltage (ECV) measurements were conducted on the annealed samples after an Hydrofluoric acid (HF) dip to remove the native or grown oxide on the surface. ECV measurements were performed using a WEP CVP21 profiler with a 0.1M solution of NH<sub>4</sub>F. The etch area was corrected based on external etch area

measurements. In this study, the carrier concentration measured by ECV is supposed to be equivalent to the electrically active [B].

**Textured samples** were used to investigate the carrier recombination activity of BLII and PIII boron emitters. For this purpose, nine batches of samples were studied, namely, BLII\_C, BLII\_D, and BLII\_E for BLII implantation and PIII\_C to PIII\_J for PIII samples. The process details of each batch are summarized in Table 2.

Samples were processed from n-type Cz 239-cm<sup>2</sup> wafers of 3 to 5 Ω.cm resistivity (sister wafers were used, from the same part of the ingot). They were first randomly textured and cleaned with an RCA step. In the three BLII batches, B<sup>+</sup> ions were implanted on both sides with a dose of  $2 \times 10^{15}$  at/cm<sup>2</sup> while the six PIII batches were implanted on both sides using a B<sub>2</sub>H<sub>6</sub> plasma and an implantation dose of  $5 \times D_1$ . Both implantation conditions were chosen to reach similar emitter sheet resistance ( $R_{sheet}$ ) of approximately 90 Ω/sq after an annealing at 1050°C. In total, three annealing schemes were tested for each implantation technique with a plateau of 5 minutes at 1050°C, of 15 minutes at 1000°C, and of 30 minutes at 950°C. The annealing also includes an in situ thermal oxidation step at the end at 720°C. It was followed by an HF dip to remove the silicon oxide. In addition, samples from three batches (PIII\_H, PIII\_I, and PIII\_J) were further etched before passivation. The etching process consists in an oxidation of the surface by an additional and longer thermal oxidation, followed by an HF dip to etch the formed SiO<sub>x</sub> layer. The oxidation time was adjusted to etch 50 to 60 nm of the emitter. All the samples were then passivated by 5 nm of Al<sub>2</sub>O<sub>3</sub> deposited on each side by thermal atomic layer deposition (ALD) and 70 nm of SiN<sub>x</sub>:H deposited by plasma-enhanced chemical vapor deposition (PECVD).

Electrical performances were assessed after an infrared (IR) firing in a belt furnace by the inductively coupled quasi-steady-state photoconductance decay method (IC-QssPC) on a Sinton WCT-120 lifetime tester. Implied open-circuit voltage ( $iV_{oc}$ ) was acquired at one sun, and the  $J_{0e}$  was extracted from the carrier lifetime measurement with the method used on the WCT-120<sup>19</sup> based on the intrinsic lifetime parametrization by Richter et al<sup>20</sup> and on the band-gap-narrowing model from Schenk.<sup>21</sup> It was applied on an injection density ( $\Delta n$ ) range of 30% of  $2 \times 10^{16}$ /cm<sup>3</sup>. The active [B] was then obtained by ECV profiling after an HF dip to remove the passivation layers. The

**TABLE 1** Summary of the processes performed on the samples together with the extracted oxide thickness and measured  $R_{sheet}$  values

Sample Name	Substrate	Implant	Implantation Dose (at/cm <sup>3</sup> )	Annealing Temperature (°C)	Oxidation Step	Oxide Thickness (nm)	$R_{sheet}$ (Ω/sq)
BLII_asImp	n-type	BLII: B <sup>+</sup>	$1.2 \times 10^{15}$	-	-	-	-
BLII_A	Cz 239-cm <sup>2</sup> wafers	BLII: B <sup>+</sup>	$1.2 \times 10^{15}$	1050	Yes	12	101
BLII_B		BLII: B <sup>+</sup>	$1.2 \times 10^{15}$	950	Yes	11	111
PIII_asImp	KOH polished	PIII: B <sub>2</sub> H <sub>6</sub>	D <sub>0</sub>	-	-	-	-
PIII_A		PIII: B <sub>2</sub> H <sub>6</sub>	D <sub>0</sub>	1050	Yes	15	79
PIII_B		PIII: B <sub>2</sub> H <sub>6</sub>	D <sub>0</sub>	950	Yes	14	145
PIII_C		PIII: B <sub>2</sub> H <sub>6</sub>	$3 \times D_0$	950	Yes	15	112
PIII_D		PIII: B <sub>2</sub> H <sub>6</sub>	$3 \times D_0$	950	No	4	106

Abbreviations: BLII, beamline ion implantation; PIII, plasma-immersion ion implantation.

**TABLE 2** Summary of the processes performed on the nine samples batches together with the average  $R_{\text{sheet}}$ 

Batch Name	Substrate	Implant	Implantation Dose (at/cm <sup>3</sup> )	Annealing Temperature (°C)	Oxidation Step	Etching	$R_{\text{sheet}}$ (Ω/sq)
BLII_C	n-type	BLII: B <sup>+</sup>	$2 \times 10^{15}$	1050	Yes	No	97
BLII_D	Cz 239-cm <sup>2</sup> wafers	BLII: B <sup>+</sup>	$2 \times 10^{15}$	1000	Yes	No	104
BLII_E		BLII: B <sup>+</sup>	$2 \times 10^{15}$	950	Yes	No	112
PIII_E	3-5 Ω.cm	PIII: B <sub>2</sub> H <sub>6</sub>	$5 \times D_1$	1050	Yes	No	89
PIII_F	KOH textured	PIII: B <sub>2</sub> H <sub>6</sub>	$5 \times D_1$	1000	Yes	No	122
PIII_G		PIII: B <sub>2</sub> H <sub>6</sub>	$5 \times D_1$	950	Yes	No	180
PIII_H		PIII: B <sub>2</sub> H <sub>6</sub>	$5 \times D_1$	1050	Yes	Yes	93
PIII_I		PIII: B <sub>2</sub> H <sub>6</sub>	$5 \times D_1$	1000	Yes	Yes	129
PIII_J		PIII: B <sub>2</sub> H <sub>6</sub>	$5 \times D_1$	950	Yes	Yes	203

Abbreviations: BLII, beamline ion implantation; PIII, plasma-immersion ion implantation.

ECV profiles were acquired using an area factor of 1.64 on these textured samples. The ECV profiles were then corrected by modifying the area factor until the calculated sheet resistance of the ECV doping profile matches the emitter sheet resistance measured by the four-point probe method.

At last, the impact of the implantation/annealing conditions on the metal/c-Si contact resistance of these emitters was investigated. A standard commercial Ag/Al paste was screen printed on the samples from the PIII batches, and the contact resistivity was assessed by the transmission line model (TLM) technique<sup>22</sup> on a GP Solar tool after an IR firing step.

Additional symmetrical SiN<sub>x</sub>/Al<sub>2</sub>O<sub>3</sub>/p<sup>+</sup>/n/p<sup>+</sup>/Al<sub>2</sub>O<sub>3</sub>/SiN<sub>x</sub> samples were similarly processed to compare several emitter sheet resistances. They were implanted by PIII from a B<sub>2</sub>H<sub>6</sub> plasma at various implantation doses from  $0.8 \times D_0$  to  $5.5 \times D_0$ . Samples were later annealed with peak temperatures ranging from 920°C to 1050°C. In this study, the oxidation step was removed from the annealing on three batches: batches PIII\_α2, PIII\_β2, and PIII\_γ2.

## 2.2 | Solar cells process

n-type PERT solar cells fully (front and rear surfaces) doped by PIII were fabricated following two industrial process flows, noted “separated anneals” and “coanneal.” For these two process flows, n-type Cz wafers (resistivity ~1 Ω.cm) were first textured in a KOH solution, followed by an RCA cleaning. Boron was then implanted on the front side by PIII from B<sub>2</sub>H<sub>6</sub> plasma, and phosphorus was implanted on the back side also by PIII but from a PH<sub>3</sub> plasma. In the coanneal case, boron and phosphorus dopants were activated in a single thermal process performed in a horizontal oxidation furnace with a high-temperature step at 950°C under N<sub>2</sub>, followed by an in situ thermal oxidation step. In the separated anneals process, a first anneal at 1000°C or 950°C including an in situ thermal oxidation was used to activate the boron dopants, and then, a second anneal with a peak temperature below 900°C in N<sub>2</sub> atmosphere was used for the phosphorus dopants. The boron implantation dose was adjusted to obtain an  $R_{\text{sheet}}$  close to 110 Ω/sq after both 950°C and

1000°C anneals. And the phosphorus implantation dose was chosen to obtain a back surface field (BSF)  $R_{\text{sheet}}$  of 45 Ω/sq after the coannealing at 950°C and a 90-Ω/sq BSF in the separated anneals process. The boron-doped emitter was passivated by an Al<sub>2</sub>O<sub>3</sub>/SiN<sub>x</sub> stack, and the phosphorus-doped BSF was passivated by a SiN<sub>x</sub> layer. The metallization grids were screen printed on each side with commercial Ag/Al and Ag pastes on the front and rear sides, respectively, with four full bus bars. The results of two batches are reported: the first with a nonspecifically optimized metallization grid leading to fingers widths of 50 to 55 μm and the second with a first optimization level leading to fingers widths of 45 μm, both widths measured after firing. The solar cells were finally fired in an IR belt furnace followed by a laser junction opening.

## 3 | RESULTS AND DISCUSSION

### 3.1 | Comparison of BLII and PIII boron emitters

#### 3.1.1 | Boron activation: Results on polished samples

As previously mentioned, BICs, inactive boron, or other extended defects can be found in the implanted boron emitter after the activation annealing, when the thermal budget is not high enough. With the goal to see if there are some variations in the inactive boron quantity between BLII and PIII techniques, SIMS and ECV analyses were compared. Two thermal anneals were studied: the first with a peak temperature at 1050°C and the second at 950°C. Table 1 summarizes the eight samples investigated for this purpose with the oxide thickness extracted from the oxygen signal of the SIMS measurement and the emitter  $R_{\text{sheet}}$  measured by the four-point probe method.

In the BLII case, the B<sup>+</sup> ion implantation dose conducts to an emitter sheet resistance of 101 Ω/sq after an anneal at 1050°C and to 111 Ω/sq after an anneal at 950°C; both anneals include an oxidation step. The boron distribution measured by SIMS after implantation can be seen in Figure 1 with the BLII\_asImp sample. The [B] profiles extracted from the SIMS and ECV measurements after the heat treatments at 1050°C and 950°C are shown in Figure 2.

As seen in Figure 2A, the SIMS and ECV measurements of [B] for the sample annealed at 1050°C are identical. This indicates the possibility of a full activation of the implanted boron in this 101 Ω/sq BLII emitter because of the absence of differences between the activated and the total [B] profiles.

In Figure 2B, it can be seen that lowering the activation temperature to 950°C introduces a gap between the SIMS and ECV curves for depths ranging from 30 to 100 nm. The space between both curves corresponds to the inactive boron dose. As previously discussed, this inactive boron dose seems to be explained by the presence of BICs in the emitter.<sup>13,14</sup> It was reported that the BICs are rapidly formed at the beginning of the annealing and once grown become immobile and hard to dissolve during further anneals.<sup>23</sup> The good correlation between the location of the inactive boron of sample BLII\_B and the region where the as-implanted [B] (BLII\_asImp curve in Figure 2B) exceeds the boron solubility limit at 950°C (ie,  $\sim 9 \times 10^{19}/\text{cm}^3$ ),<sup>24</sup> further supports the immobile BICs hypothesis. For comparison, the solubility limit<sup>24</sup> at 1050°C is of  $1.5 \times 10^{20}/\text{cm}^3$ .

The case of PIII boron emitters can be discussed with PIII\_A and PIII\_B samples of Table 1, also characterized in Figure 3. The implantation dose  $D_0$  used on these PIII emitters results in an  $R_{\text{sheet}}$  of 79 Ω/sq after the anneal at 1050°C and in an  $R_{\text{sheet}}$  of 145 Ω/sq at 950°C. A stronger increase of  $R_{\text{sheet}}$  can be noted with the annealing temperature decrease to 950°C on these PIII emitters as compared with the previous BLII case.

Similarly to the BLII boron emitter, the perfect matching between SIMS and ECV curves at 1050°C (see Figure 3A) suggests a complete activation of the boron atoms in the emitter. If BLII\_A and PIII\_A are indeed fully activated, the lower  $R_{\text{sheet}}$  measured on the PIII emitter (79 Ω/sq instead of 101 Ω/sq) means that the  $D_0$  dose used for the PIII sample corresponds to a higher boron-implanted dose than the  $1.2 \times 10^{15}\text{-at}/\text{cm}^2$  dose of the BLII sample.

At 950°C in Figure 3B however, the SIMS curve of PIII\_B differs from the BLII\_B sample, as the bump between 30 to 100 nm of depth is no longer seen. A good correlation between the SIMS and ECV curves is observed for PIII\_B despite the low annealing temperature. The PIII as-implanted profile is also displayed on Figure 3B to locate the region where [B] exceeds the solubility limit of boron at 950°C and thus where the BICs are the most likely to be formed. The PIII as-implanted boron distribution only exceeds  $9 \times 10^{19}/\text{cm}^3$  in the first 15 nm of the profile. As a result of the in situ oxidation step, most of this area will be after the activation annealing step located inside the 14 nm of  $\text{SiO}_2$  layer and not inside the emitter. This is a major difference with the BLII technique where the as-implanted [B] exceeds the solubility limit at 950°C much deeper in the wafer (from 10 to 70 nm). In the PIII emitter annealed at 950°C, the “near-surface” location of the as-implanted maximum concentration and the growth of the silicon oxide that consumes most of the area where [B] exceeds the solubility limit could explain the absence of BICs and consequently the full activation of the B atoms within the emitter observed in Figure 3B. Even if the high voltage used for the PIII implantation increases, according to the as-implanted profile, the location where [B] exceeds its 950°C solubility limit remains very close to the surface (see Figure 1 for the variation between 4 and 8 kV).

As the  $R_{\text{sheet}}$  of this PIII\_B sample is higher than the BLII\_B sample, 145 Ω/sq instead of 111 Ω/sq, the implantation dose of PIII boron emitter was increased to  $3 \times D_0$  in samples PIII\_C and PIII\_D in order to compare emitters of similar  $R_{\text{sheet}}$ . SIMS and ECV measurements of PIII\_C sample annealed at 950°C and with a lower  $R_{\text{sheet}}$  of 112 Ω/sq are displayed on Figure 4A. Despite the increase of the PIII implantation dose that could enhance the possibility of BICs formation, a perfect matching of the SIMS and ECV curves is still observed for an emitter  $R_{\text{sheet}}$  of 112 Ω/sq.

Finally, the impact of the silicon oxide growth on the total and electrically active [B] was studied with sample PIII\_D, similarly processed than PIII\_C, but without the oxidation step. Without the oxidation step, the main impact on the total [B] profile (see Figure 4B) is the absence of the boron depletion previously observed at the  $\text{SiO}_2/\text{Si}$  interface on the PIII\_C sample. Moreover, without the oxidation step, in the first 20 nm below the surface, a gap between the SIMS and ECV curves can be observed that suggests the presence of inactive boron atoms in this area. The oxidation step seems then to be necessary to form a fully activated PIII boron emitter annealed at 950°C.

### 3.1.2 | Carrier recombination activity of the implanted boron emitters: Results on textured samples

The variation of the boron emitter recombination activity between BLII and PIII techniques was investigated with nine different boron emitters with features summarized in Table 2, all passivated by an  $\text{Al}_2\text{O}_3/\text{SiN}_x$  stack. The implantation dose was kept constant in this part for each implantation technique, and three annealing schemes were studied with peak temperatures at 1050°C, 1000°C, and 950°C. The two implants result in similar  $R_{\text{sheet}}$  after the 1050°C anneal with 89 and 97 Ω/sq for PIII\_E and BLII\_C emitters, respectively. Lowering the temperature from 1050°C to 950°C increases the  $R_{\text{sheet}}$  in all cases.

The activated [B] profiles of the emitters described in Table 2 are shown in Figure 5. For BLII emitters (see Figure 5A), shorter junction depths and higher maximal [B] are observed for lower annealing temperatures.

Regarding the PIII-related active [B] profiles (see Figure 5B), the maximum activated concentration is constant for all the annealing temperatures along with shorter junction depths for lower annealing temperatures, reminiscent of the [B] profiles after an indiffusion from a deposited doped layer.<sup>25</sup> Consequently, the total activated boron dose (integral of the ECV curve) strongly reduces in PIII between the 1050°C and the 950°C anneal with  $1.2 \times 10^{15}$  and  $5.9 \times 10^{14}$  at/cm<sup>2</sup>, respectively. This drop of boron dose can explain the large increase of  $R_{\text{sheet}}$  measured when the temperature decreases in the PIII case (see Tables 1 and 2). The missing boron dose at 950°C does not seem to be in an inactive state, as the SIMS concentration profile in Figure 4A shows a full activation of the emitter. We can however suspect that the missing dose is located inside the  $\text{SiO}_2$  layer as a higher [B] is measured inside it at 950°C than at 1050°C in Figure 3.

The  $iV_{\text{oc}}$  and  $J_{\text{0e}}$  measured on the boron emitters of Table 2 are displayed in Figure 6. For a 1050°C peak temperature, similar  $J_{\text{0e}}$  and



$iV_{oc}$  values are determined for both implantation techniques, with  $J_{0e}$  below 35 fA/cm<sup>2</sup> and  $iV_{oc}$  above 685 mV. However, at lower annealing temperatures, different behaviors are observed between PIII and BLII boron emitters. In agreement with the literature, for the BLII of B<sup>+</sup> ions, a strong drop in the  $iV_{oc}$  value is observed when the temperature reduces from 1050°C to 950°C, together with a large increase of the  $J_{0e}$ . As reported before<sup>15,26</sup> and confirmed with this work (Figure 2), it mainly results from a higher inactive [B].

A completely different trend is observed for PIII boron emitters where there is no degradation of the emitter quality for annealing at 1000°C and 950°C compared with the 1050°C case. A measurable improvement can even be noticed for temperatures below 1050°C for both parameters,  $iV_{oc}$  and  $J_{0e}$ . Further etching of the emitter (removing 50–60 nm as seen in Figure 5B) before passivation only slightly improves the  $J_{0e}$  values. This is in agreement with the absence of implanted defects and a full activation of the boron in these PIII-doped emitters from B<sub>2</sub>H<sub>6</sub> plasma even if annealed at 950°C.

### 3.2 | Impact of the implantation dose on the PIII boron emitters properties

In the above results, the PIII boron emitter quality was measured at 950°C only for a high-emitter  $R_{sheet}$  of 180 Ω/sq. For a more accurate assessment of the PIII boron-doped emitters, the  $R_{sheet}$  was varied by changing the implantation dose for several annealing schemes. The implantation doses used for each annealing peak temperature are detailed below.

- At 1050°C, implantation doses ranging from  $0.8 \times D_0$  to  $1.6 \times D_0$  at/cm<sup>2</sup> were used, resulting in  $R_{sheet}$  variations from 156 to 101 Ω/sq.

- At 1000°C, implantation doses ranging from  $1.1 \times D_0$  to  $2.2 \times D_0$  at/cm<sup>2</sup> were used resulting in  $R_{sheet}$  variations from 157 to 110 Ω/sq.
- At 975°C, implantation doses ranging from  $1.6 \times D_0$  to  $2 \times D_0$  at/cm<sup>2</sup> were used resulting in  $R_{sheet}$  variations from 157 to 144 Ω/sq.
- At 950°C, implantation doses ranging from  $2 \times D_0$  to  $5.5 \times D_0$  at/cm<sup>2</sup> were used resulting in  $R_{sheet}$  variations from 178 to 124 Ω/sq. Finally, the implantation dose  $5.5 \times D_0$  at/cm<sup>2</sup> corresponding to an  $R_{sheet}$  of 185 Ω/sq was performed with a peak temperature of 920°C.

The corresponding  $iV_{oc}$  and  $J_{0e}$  measurements are shown in Figure 7. Looking first at the  $J_{0e}$  results, very low values, below 21 fA/cm<sup>2</sup>, were measured for annealing temperature at 975°C and above. This highlights and confirms the very high quality of these boron emitters, with a likely full recovery of implantation defects and that for all the implantation doses studied and  $R_{sheet}$  from 100 to 160 Ω/sq.

In the case of an annealing at 950°C, the lowest  $J_{0e}$  value of 13 fA/cm<sup>2</sup> was determined for a 178 Ω/sq emitter with a corresponding  $iV_{oc}$  value of 706 mV. While raising the implantation dose to  $5.5 \times D_0$  ( $R_{sheet}$  of 124 Ω/sq), an increase of  $J_{0e}$  is observed at 950°C that could be due to the remaining of some implantation damages for this high implantation dose or to the increasing contribution of Auger recombination in the emitter with the higher boron concentration (see Figures 3B and 4A as example of the boron concentration increase with higher implantation dose). Auger contribution to the  $J_{0e}$  value was simulated on PV Lighthouse EDNA 2 calculator<sup>27</sup> using the active [B] profile measured by ECV of these 950°C annealed emitters with  $R_{sheet}$  of 178 and 124 Ω/sq. The latest Auger parameterization by Richter et al<sup>28</sup> was

**TABLE 3**  $R_{sheet}$ ,  $J_{0e}$ , and the simulated contribution of Auger recombination to the  $J_{0e}$  value noted  $J_{0e\_Auger}$  of PIII boron-doped emitters annealed at 950°C

Implant	Implantation Dose (at/cm <sup>3</sup> )	Annealing Temperature (°C)	$R_{sheet}$ (Ω/sq)	$J_{0e}$ (fA/cm <sup>2</sup> )	$J_{0e\_Auger}$ (fA/cm <sup>2</sup> )	$J_{0e\_Auger}$ (%)
PIII: B <sub>2</sub> H <sub>6</sub>	$2.0 \times D_0$	950	178	13	9.0	69
PIII: B <sub>2</sub> H <sub>6</sub>	$5.5 \times D_0$	950	124	54	16.8	31

Abbreviation: PIII, plasma-immersion ion implantation.

**TABLE 4**  $R_{sheet}$ ,  $iV_{oc}$ , and  $J_{0e}$  values of PIII boron-doped emitters passivated by an Al<sub>2</sub>O<sub>3</sub>/SiN<sub>x</sub> stack with and without the in situ oxidation step during the boron activation annealing

Name	Implant	Implantation Dose (at/cm <sup>3</sup> )	Annealing Temperature (°C)	Oxidation Step	$R_{sheet}$ (Ω/sq)	$iV_{oc}$ (mV)	$J_{0e}$ (fA/cm <sup>2</sup> )
PIII_α1	PIII: B <sub>2</sub> H <sub>6</sub>	$3.5 \times D_1$	1050	Yes	101	693	20
PIII_α2	PIII: B <sub>2</sub> H <sub>6</sub>	$3.5 \times D_1$	1050	No	97	677	25
PIII_β1	PIII: B <sub>2</sub> H <sub>6</sub>	$4.8 \times D_1$	1000	Yes	110	696	18
PIII_β2	PIII: B <sub>2</sub> H <sub>6</sub>	$4.8 \times D_1$	1000	No	106	688	28
PIII_γ1	PIII: B <sub>2</sub> H <sub>6</sub>	$12 \times D_1$	950	Yes	124	676	54
PIII_γ2	PIII: B <sub>2</sub> H <sub>6</sub>	$12 \times D_1$	950	No	116	651	166

Abbreviation: PIII, plasma-immersion ion implantation.

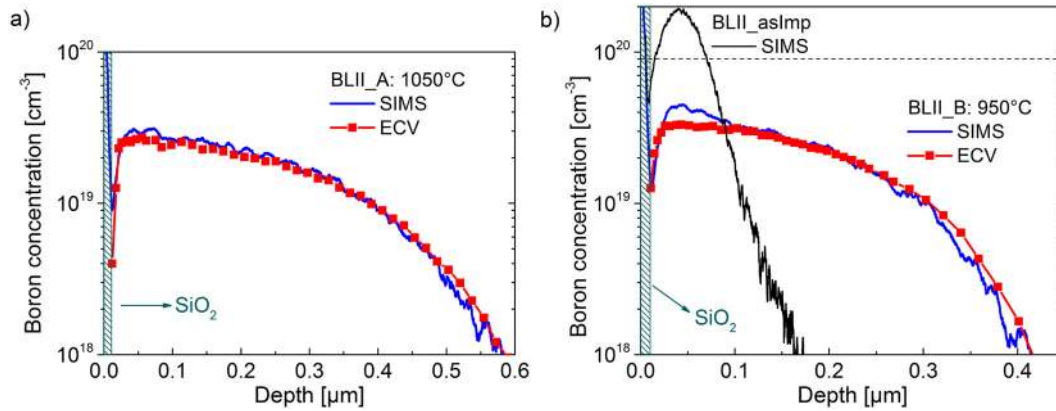


**FIGURE 2** Boron concentration measured by secondary-ion mass spectroscopy (SIMS) and activated boron concentration obtained by electrochemical capacitance voltage (ECV) measurement of A, sample BLII\_A and B, sample BLII\_B, both detailed in Table 1. SIMS was performed after the annealing and oxidation step, and ECV was performed after an additional HF dip. SiO<sub>2</sub> thickness is represented with the hatched area, and the SIMS of the BLII\_aslmp sample was added in B, for comparison along with the boron solubility limit at 950°C as a dot line at  $9 \times 10^{19}/\text{cm}^3$  [Colour figure can be viewed at wileyonlinelibrary.com]

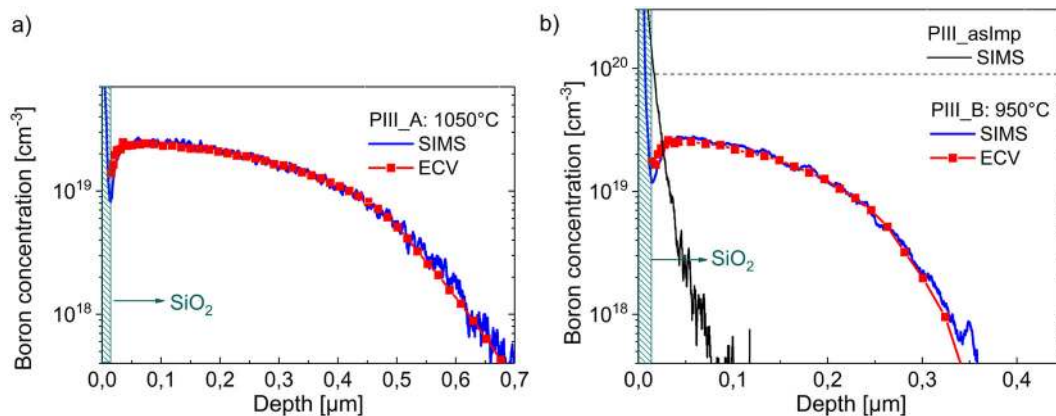


**FIGURE 3** Boron concentration measured by secondary-ion mass spectroscopy (SIMS) and activated boron concentration obtained by electrochemical capacitance voltage (ECV) measurement of A, sample PIII\_A and B, sample PIII\_B, both detailed in Table 1. SIMS was performed after the annealing and oxidation step, and ECV was performed after an additional HF dip. SiO<sub>2</sub> thickness is represented with the hatched area. The SIMS measurement of the PIII\_aslmp sample was added in B, for comparison along with the boron solubility limit at 950°C as a dot line at  $9 \times 10^{19}/\text{cm}^3$  [Colour figure can be viewed at wileyonlinelibrary.com]

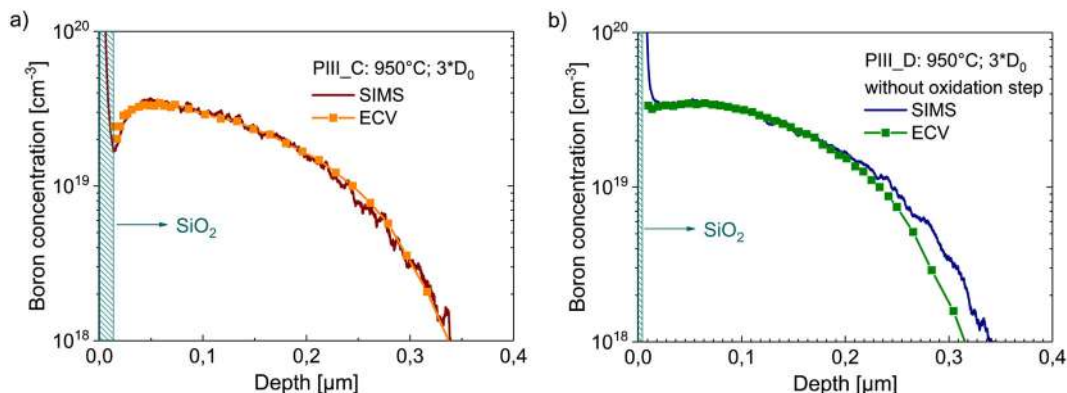


**FIGURE 4** Boron concentration measured by secondary-ion mass spectroscopy (SIMS) and activated boron concentration obtained by electrochemical capacitance voltage (ECV) measurement of A, sample PIII\_C and B, sample PIII\_D, both detailed in Table 1. SIMS was performed after the annealing and oxidation step, and ECV was performed after an additional HF dip. SiO<sub>2</sub> thickness is displayed with the hatched area [Colour figure can be viewed at wileyonlinelibrary.com]



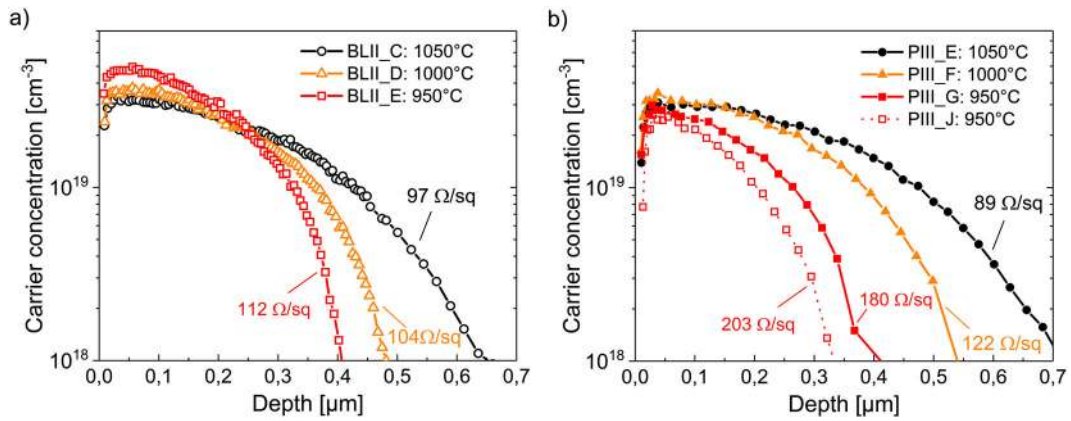


**FIGURE 5** Electrochemical capacitance voltage (ECV) measurements of A, beamline ion implantation (BLII) and B, plasma-immersion ion implantation (PIII) boron-doped emitters annealed at 950°C (30 min), 1000°C (15 min), and 1050°C (5 min), with corresponding sheet resistances. The case of PIII\_J emitter annealed at 950°C and further etched is added in B, [Colour figure can be viewed at wileyonlinelibrary.com]

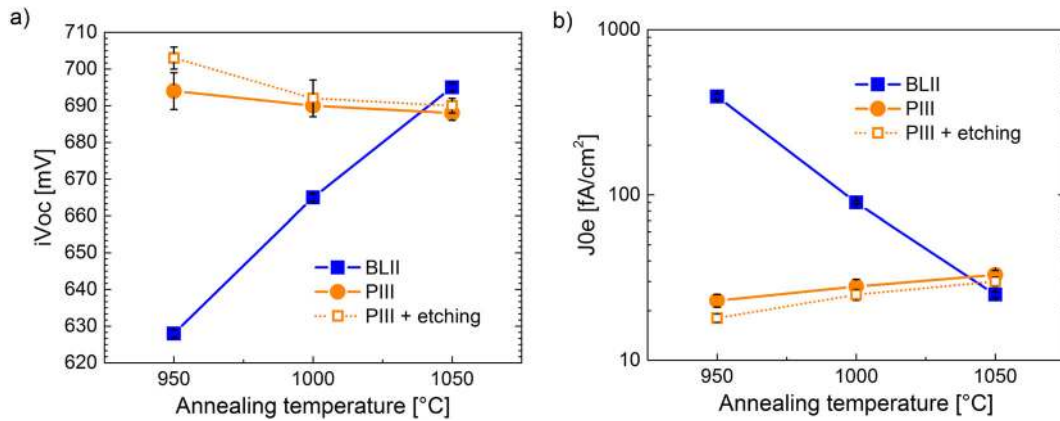


**FIGURE 6** A,  $iV_{oc}$  and B,  $J_{0e}$  average and distribution determined on the boron-implanted emitters detailed in Table 2. Plasma-immersion ion implantation (PIII) and beamline ion implantation (BLII) comparison for annealing at 1050°C (5 min), 1000°C (15 min), or 950°C (30 min) using an  $Al_2O_3/SiN_x$  passivation, with or without an additional 50- to 60-nm etching step in the PIII case

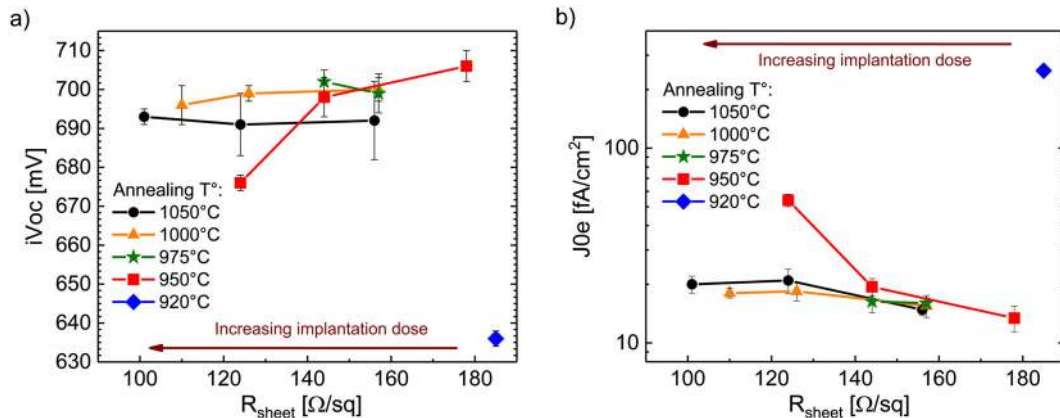


**FIGURE 7** (A)  $iV_{oc}$  and (B)  $J_{0e}$  average values of plasma-immersion ion implantation (PIII) boron emitters annealed at various annealing peak temperatures and time with  $Al_2O_3/SiN_x$  passivation. Several implantation doses were used increasing from  $0.8 \times 10^{15}$  to  $5.5 \times 10^{15}$  at/cm<sup>2</sup> [Colour figure can be viewed at wileyonlinelibrary.com]

used while deactivating the “SRH-at-surface” and “SRH-in-emitter” module. Simulation results are shown in Table 3. The  $J_{0e}$  only due to Auger recombination increases from 9.0 to 16.8 fA/cm<sup>2</sup> when the implantation dose increases from  $2.0 \times D_0$  to  $5.5 \times D_0$ . However, the  $J_{0e}$  increase due to Auger recombination only represents 19.0% of the total  $J_{0e}$  increase (increase from 13 to 54 fA/cm<sup>2</sup>). Therefore, 81.0% of the  $J_{0e}$  increase would be related to Shockley-Read-Hall (SRH) recombination in the emitter or at the surface, likely to be due to remaining implantation damages for the high implantation dose.

Finally, the PIII boron-doped emitter annealed at 920°C exhibits a very high  $J_{0e}$  value above 200 fA/cm<sup>2</sup> for a sheet resistance of 185 Ω/sq, which is not suitable for solar cells processing, and suggests stable BICs formation in the emitter.

A good correlation of the  $iV_{oc}$  results with the  $J_{0e}$  values is seen in Figure 7 with a strong degradation of the  $iV_{oc}$  at 920°C and lower performances of the  $iV_{oc}$  for the highest dose used with the annealing at 950°C. Lower  $iV_{oc}$  performances are measured at 1050°C as compared with 1000°C and 975°C anneals that could result from a bulk carrier lifetime deterioration due to the high-thermal budget. This hypothesis is supported by a decrease of the estimated bulk lifetime extracted from the IC-QssPC measurements, from 700 to 580 μs when the annealing temperature increases from 1000°C to 1050°C. The  $iV_{oc}$  decrease highlights the necessity to lower the annealing temperature below 1050°C to avoid the bulk degradation and thus reach higher efficiencies.

At last, the effect of the oxidation step during the activation annealing on the emitter quality was investigated in Table 4. For each annealing peak temperature, a slight increase of the  $R_{sheet}$  is measured with the oxidation step, which is explained by the emitter

consumption during the SiO<sub>2</sub> growth (see Figure 4 that illustrates the impact on the [B] profile).

Results exhibit lower  $iV_{oc}$  values on the PIII boron-doped emitter when the oxidation step is removed, with drops between 8 and 25 mV. Similarly,  $J_{0e}$  values slightly increase without the oxidation but remain very low for the 1050°C and 1000°C cases. At 950°C however, the  $J_{0e}$  value of PIII\_γ2 strongly increases without oxidation and exceeds 160 fA/cm<sup>2</sup>, which is consistent with the inactive boron dose observed in the PIII boron emitter annealed at 950°C in Figure 4B. Therefore, the oxidation step is always beneficial and becomes necessary if the annealing temperature is reduced down to 950°C.

### 3.3 | Integration of PIII boron emitter in n-type PERT solar cells

#### 3.3.1 | Contact by screen printing

The contact resistivity determined on the PIII boron-doped emitter after the screen printing and firing of a commercial Ag/Al paste was investigated on all the PIII emitters from Table 2. Results shown in Table 5 confirm a good contact resistivity (below 6 mΩ.cm<sup>2</sup>) in all cases even for boron emitter sheet resistances of 180 Ω/sq with sample PIII\_G and of 203 Ω/sq for PIII\_J.

#### 3.3.2 | Full PIII-implanted n-type PERT solar cells

In this section, the PIII boron-doped emitters annealed at low temperature (950°C and 1000°C) were integrated in full PIII n-PERT

**TABLE 5** Average contact resistivity measured on six batches of PIII boron emitters detailed in Table 2

Name	Implant	Annealing Temperature (°C)	Etching	$\rho_c$ (mΩ.cm <sup>2</sup> )
PIII_E	PIII: B <sub>2</sub> H <sub>6</sub>	1050	No	2.4
PIII_F	PIII: B <sub>2</sub> H <sub>6</sub>	1000	No	2.7
PIII_G	PIII: B <sub>2</sub> H <sub>6</sub>	950	No	4.4
PIII_H	PIII: B <sub>2</sub> H <sub>6</sub>	1050	Yes	1.7
PIII_I	PIII: B <sub>2</sub> H <sub>6</sub>	1000	Yes	2.7
PIII_J	PIII: B <sub>2</sub> H <sub>6</sub>	950	Yes	5.6

Abbreviation: PIII, plasma-immersion ion implantation.

**TABLE 6** I(V) parameters of champion n-PERT solar cells fully doped by PIII using the separate anneals and coanneal processes

Process	Boron Annealing Temperature (°C)	Emitter $R_{sheet}$ (Ω/sq)	$V_{oc}$ (mV)	$J_{sc}$ (mA/cm <sup>2</sup> )	FF (%)	$\eta$ (%)
Separated anneals—batch 1	1000	110	660 <sup>a</sup>	39.3 <sup>a</sup>	79.4 <sup>a</sup>	20.6 <sup>a</sup>
Separated anneals—batch 2	1000	100	665	39.5	79.1	20.8
	950	122	662	39.5	79.0	20.7
Coanneal—batch 2	950	115	660	39.5	79.2	20.7

Note. The corresponding  $R_{sheet}$  of the boron emitter is also indicated.

Abbreviations: PERT, passivated emitter rear totally diffused; PIII, plasma-immersion ion implantation.

<sup>a</sup>Measure independently confirmed at CalTec.

solar cells. The complete industrial process flows noted as separated anneals and detailed above were used for these cells, with two successive batches. For the first batch (batch 1), a single-layer antireflective coating was used as well as a nonspecifically optimized metallization grid, leading to large finger widths of 50 to 55  $\mu\text{m}$  after firing. The second (batch 2) includes improvements on the metallization process (with finger widths of 45  $\mu\text{m}$  after firing) and a double-layer antireflective coating. Champion cells (V) parameters of each process are reported in Table 6.

In the first batch, a maximum efficiency of 20.6% (independently confirmed by CalTec) was measured using two anneals to separately activate boron and phosphorus dopants with an annealing temperature below 1050°C for the boron activation. The high performance of the boron emitter annealed at 1000°C is supported by the high open-circuit voltage ( $V_{oc}$ ) value of 660 mV and the efficiency of 20.6% close to the current n-PERT performances found in pilot lines.<sup>3</sup> As the efficiency is mainly limited on these cells by the short-circuit current density ( $J_{sc}$ ), work on the metallization grid was performed to increase this parameter with batch 2.

In batch 2, two annealing temperatures were compared for the boron activation, 1000°C and 950°C, leading to boron emitter  $R_{sheet}$  of 100 and 122  $\Omega/\text{sq}$ , respectively. At 1000°C, the boron emitter corresponds to a  $J_{0e}$  value of 22  $\text{fA}/\text{cm}^2$ , measured on symmetrical samples. In that case, solar cell results show a maximum efficiency of 20.8% because of the improvement of the  $V_{oc}$  up to 665 mV and of the  $J_{sc}$ . This  $J_{sc}$  value is expected to increase even further with additional optimization of the metallization process. The use of a lower anneal temperature of 950°C in this separated anneals process leads to similar performance to the 1000°C anneal with a maximum solar cell efficiency of 20.7%, despite an expected slight increase of the  $J_{0e}$  value just as observed in Figure 7B for this  $R_{sheet}$  of 122  $\Omega/\text{sq}$ . This is an important result that confirms the above study at the solar cell scale, especially the  $V_{oc}$  value above 660 mV demonstrates the possibility to anneal boron-implanted emitters at 950°C while using PIII implantation from  $\text{B}_2\text{H}_6$  plasma.

In addition, solar cells were processed with a single annealing at 950°C to activate both dopants. Result of this coanneal process shows for the first time similar performances than the separated anneals cells, with the same maximum efficiency of 20.7%, contrary to previous work where lower efficiencies were reported with the coannealed process at 1050°C.<sup>7</sup> Therefore, lowering the activation temperature down to 950°C not only avoids bulk carrier lifetime degradations from high-thermal treatments but also increases the efficiency potential of this ultrasimplified co-anneal process flow. Combined with the reduced production cost of the PIII technique, this process becomes a promising candidate for n-PERT solar cells fabrication.

## 4 | CONCLUSION

We report on a new way of activating the implanted boron emitter at temperatures below 1050°C based on the use of PIII from  $\text{B}_2\text{H}_6$  plasma instead of the standard BLII of  $\text{B}^+$  ions. Because of the differences in the

as-implanted profile (maximum concentration of boron located at the surface in PIII), PIII boron-doped emitters without implantation damages and boron clusters were obtained with annealing temperature down to 950°C. A full activation of the emitter at 950°C was observed even for a high implantation dose corresponding to a sheet resistance of 112  $\Omega/\text{sq}$ . The results also highlight the important role of the oxidation step subsequent to the activation annealing to avoid the presence of inactive boron atoms in the emitter. At 1000°C,  $J_{0e}$  below 21  $\text{fA}/\text{cm}^2$  was obtained using the PIII technique regardless of the implantation dose for sheet resistances between 110 and 160  $\Omega/\text{sq}$ , while  $J_{0e}$  increases above 85  $\text{fA}/\text{cm}^2$  for BLII emitter of 104  $\Omega/\text{sq}$ . The PIII boron emitters show promising performances while being integrated into n-PERT solar cells fully doped by PIII with efficiency of 20.6% independently confirmed. Furthermore, an efficiency of 20.7% was obtained with an ultrasimplified n-PERT process flow, including two low-cost PIII implantations and a single coannealing at 950°C.

## ACKNOWLEDGEMENTS

The authors would like to thank E. De Vito from CEA Leti for the SIMS measurements and analyses and the Bpifrance and FUI for their financial support through the French ISICELL project.

## ORCID

Adeline Lanterne  <https://orcid.org/0000-0001-8080-2545>

## REFERENCES

1. Min B, Muller M, Wagner H, et al. A roadmap toward 24% efficient PERC solar cells in industrial mass production. *IEEE J Photovoltaics*. 2017;7(6):1541-1550.
2. "International Technology Roadmap for Photovoltaic (ITRPV) 2016 results including maturity report," www.itrpv.net, no. September, 2017.
3. Buchholz F, Preis P, Chu H, Lossen J, Wehringhaus E. Progress in the development of industrial nPERT cells. *Energy Procedia*. 2017;124:649-656.
4. Ryu K, Cho E, Rohatgi A, Ok Y-W. Process development and comparison of various boron emitter technologies for high-efficiency (~21%) n-type silicon solar cells. *Prog Photovolt Res Appl*. 2016;24(8):1109-1115.
5. Das A, Ryu K, Rohatgi A. 20% efficient screen-printed n-type solar cells using a spin-on source and thermal oxide/silicon nitride passivation. *IEEE J Photovoltaics*. 2011;1(2):146-152.
6. Lim B, Brendemuhl T, Dullweber T, Brendel R. Loss analysis of n-type passivated emitter rear totally diffused back-junction silicon solar cells with efficiencies up to 21.2%. *IEEE J Photovoltaics*. 2016;6(2):447-453.
7. Kiefer F, Krügener J, Heinemeyer F, et al. Bifacial, fully screen-printed n-PERT solar cells with BF2 and B implanted emitters. *Sol Energy Mater Sol Cells*. 2016;157:326-330.
8. Wei Q, Zhang S, Yu S, Lu J, Lian W, Ni Z. High efficiency n-PERT solar cells by B/P co-diffusion method. *Energy Procedia*. 2017;124:700-705.
9. Ryu K, Madani K, Rohatgi A, Ok YW. High efficiency screen-printed n-type silicon solar cell using co-diffusion of APCVD boron emitter and POC13 back surface field. *Curr Appl Phys*. 2018;18(2):231-235.
10. Low RJ, Gupta A, Bateman N, et al. "High efficiency selective emitter enabled through patterned ion implantation," *35th IEEE Photovolt. Spec. Conf.*, pp. 1440-1445, 2010.

11. Rohatgi A, Meier DL, McPherson B, et al. High-throughput ion-implantation for low-cost high-efficiency silicon solar cells. *Energy Procedia*. 2012;15:10-19.
12. Krügener J, Peibst R, Bugiel E, et al. Ion implantation of boric molecules for silicon solar cells. *Sol Energy Mater Sol Cells*. 2015;142:12-17.
13. Aboy M, Santos I, Pelaz L, Marqués LA, López P. Modeling of defects, dopant diffusion and clustering in silicon. *J Comput Electron*. 2014;13(1):40-58.
14. Raghuvanshi M, Lanterne A, le Perchec J, et al. Influence of boron clustering on the emitter quality of implanted silicon solar cells: an atom probe tomography study. *Prog Photovoltaics Res Appl*. 2015;23(12):1724-1733.
15. Müller R, Benick J, Bateman N, et al. Evaluation of implantation annealing for highly-doped selective boron emitters suitable for screen-printed contacts. *Sol Energy Mater Sol Cells*. 2014;120:431-435.
16. Müller R, Moldovan A, Schiller C, Benick J. Defect removal after low temperature annealing of boron implantations by emitter etch-back for silicon solar cells. *Phys Status Solidi—Rapid Res Lett*. 2015;9(1):32-35.
17. Desrues T, Michel T, Lerat JF, et al. "High quality industrial phosphorus emitter doping obtained with innovative plasma immersion ion implantation (PIII) processes," *Proceeding 33rd Eur. Photovolt. Sol. Energy Conf. Exhib. Amsterdam*, pp. 960-962, 2017.
18. Michel T, le Perchec J, Lanterne A, et al. Phosphorus emitter engineering by plasma-immersion ion implantation for c-Si solar cells. *Sol Energy Mater Sol Cells*. 2015;133:194-200.
19. Kimmerle A, Rothhardt P, Wolf A, Sinton RA. Increased reliability for  $J_0$ -analysis by QSSPC. *Energy Procedia*. 2014;55:101-106.
20. Richter A, Glunz SW, Werner F, Schmidt J, Cuevas A. Improved quantitative description of Auger recombination in crystalline silicon. *Phys Rev B*. 2012;86(16):165202.
21. Schenk A. Finite-temperature full random-phase approximation model of band gap narrowing for silicon device simulation. *J Appl Phys*. 2013;84(7):3684.
22. Reeves GK, Harrison HB. Obtaining the specific contact resistance from transmission line model measurements. *IEEE Electron Device Lett*. 1982;3(5):111-113.
23. De Salvador D, Napolitani E, Bisognin G, et al. Dissolution kinetics of B clusters in crystalline Si. *Mater Sci Eng B Solid-State Mater Adv Technol*. 2005;124-125:32-38.
24. Nobili D. "Properties of silicon," *EMIS Datareviews Ser. No. 4 New York INSPEC*, pp. 384-385, 1988.
25. Packan P, Thompson S, Andideh E, et al. "Modeling solid source boron diffusion for advanced transistor applications," *IEDM Tech. Dig., San Fr. CA, USA*, pp. 505-508, 1998.
26. Lanterne A, Gall S, Veschetti Y, et al. High efficiency fully implanted and co-annealed bifacial n-type solar cells. *Energy Procedia*. 2013;38:283-288.
27. "PV Lighthouse," [www.pvlighthouse.com.au](http://www.pvlighthouse.com.au), 2018.
28. Richter A, Glunz SW, Werner F, Schmidt J, Cuevas A. Improved quantitative description of Auger recombination in crystalline silicon. *Phys Rev B—Condens Matter Mater Phys*. 2012;86(16):165202.

**How to cite this article:** Lanterne A, Desrues T, Lorfèvre C, et al. Plasma-immersion ion implantation: A path to lower the annealing temperature of implanted boron emitters and simplify PERT solar cell processing. *Prog Photovolt Res Appl*. 2019;1-11. <https://doi.org/10.1002/pip.3186>